



Foreign Object Damage Behavior of Two Gas-Turbine Grade Silicon Nitrides by Steel Ball Projectiles at Ambient Temperature

Sung R. Choi
Ohio Aerospace Institute, Brook Park, Ohio

J. Michael Pereira, Lesley A. Janosik, and Ramakrishna T. Bhatt
Glenn Research Center, Cleveland, Ohio

The NASA STI Program Office . . . in Profile

Since its founding, NASA has been dedicated to the advancement of aeronautics and space science. The NASA Scientific and Technical Information (STI) Program Office plays a key part in helping NASA maintain this important role.

The NASA STI Program Office is operated by Langley Research Center, the Lead Center for NASA's scientific and technical information. The NASA STI Program Office provides access to the NASA STI Database, the largest collection of aeronautical and space science STI in the world. The Program Office is also NASA's institutional mechanism for disseminating the results of its research and development activities. These results are published by NASA in the NASA STI Report Series, which includes the following report types:

- **TECHNICAL PUBLICATION.** Reports of completed research or a major significant phase of research that present the results of NASA programs and include extensive data or theoretical analysis. Includes compilations of significant scientific and technical data and information deemed to be of continuing reference value. NASA's counterpart of peer-reviewed formal professional papers but has less stringent limitations on manuscript length and extent of graphic presentations.
- **TECHNICAL MEMORANDUM.** Scientific and technical findings that are preliminary or of specialized interest, e.g., quick release reports, working papers, and bibliographies that contain minimal annotation. Does not contain extensive analysis.
- **CONTRACTOR REPORT.** Scientific and technical findings by NASA-sponsored contractors and grantees.

- **CONFERENCE PUBLICATION.** Collected papers from scientific and technical conferences, symposia, seminars, or other meetings sponsored or cosponsored by NASA.
- **SPECIAL PUBLICATION.** Scientific, technical, or historical information from NASA programs, projects, and missions, often concerned with subjects having substantial public interest.
- **TECHNICAL TRANSLATION.** English-language translations of foreign scientific and technical material pertinent to NASA's mission.

Specialized services that complement the STI Program Office's diverse offerings include creating custom thesauri, building customized databases, organizing and publishing research results . . . even providing videos.

For more information about the NASA STI Program Office, see the following:

- Access the NASA STI Program Home Page at <http://www.sti.nasa.gov>
- E-mail your question via the Internet to help@sti.nasa.gov
- Fax your question to the NASA Access Help Desk at 301-621-0134
- Telephone the NASA Access Help Desk at 301-621-0390
- Write to:
NASA Access Help Desk
NASA Center for Aerospace Information
7121 Standard Drive
Hanover, MD 21076



Foreign Object Damage Behavior of Two Gas-Turbine Grade Silicon Nitrides by Steel Ball Projectiles at Ambient Temperature

Sung R. Choi
Ohio Aerospace Institute, Brook Park, Ohio

J. Michael Pereira, Lesley A. Janosik, and Ramakrishna T. Bhatt
Glenn Research Center, Cleveland, Ohio

National Aeronautics and
Space Administration

Glenn Research Center

Acknowledgments

The authors are thankful to R. Pawlik for the experimental work during the course of this study. This work was supported by Higher Operating Temperature Propulsion Components (HOTPC) program, NASA Glenn Research Center, Cleveland, Ohio.

This report is a formal draft or working paper, intended to solicit comments and ideas from a technical peer group.

Trade names or manufacturers' names are used in this report for identification only. This usage does not constitute an official endorsement, either expressed or implied, by the National Aeronautics and Space Administration.

The Aerospace Propulsion and Power Program at NASA Glenn Research Center sponsored this work.

Available from

NASA Center for Aerospace Information
7121 Standard Drive
Hanover, MD 21076

National Technical Information Service
5285 Port Royal Road
Springfield, VA 22100

Available electronically at <http://gltrs.grc.nasa.gov>

FOREIGN OBJECT DAMAGE BEHAVIOR OF TWO GAS-TURBINE GRADE SILICON NITRIDES BY STEEL BALL PROJECTILES AT AMBIENT TEMPERATURE

Sung R. Choi*
Ohio Aerospace Institute
Brook Park, Ohio 44142

J. Michael Pereira, Lesley A. Janosik, and Ramakrishna T. Bhatt
National Aeronautics and Space Administration
Glenn Research Center
Cleveland, Ohio 44135

ABSTRACT

Foreign object damage (FOD) behavior of two commercial gas-turbine grade silicon nitrides, AS800 and SN282, was determined at ambient temperature through strength testing of flexure test specimens impacted by steel-ball projectiles with a diameter of 1.59 mm in a velocity range from 220 to 440 m/s. AS800 silicon nitride exhibited a greater FOD resistance than SN282, primarily due to its greater value of fracture toughness (K_{IC}). Additionally, the FOD response of an equiaxed, fine-grained silicon nitride (NC132) was also investigated to provide further insight. The NC132 silicon nitride exhibited the lowest fracture toughness of the three materials tested, providing further evidence that K_{IC} is a key material parameter affecting FOD resistance. The observed damage generated by projectile impact was typically in the forms of well- or ill-developed ring or cone cracks with little presence of radial cracks.

INTRODUCTION

Ceramics, because of their brittle nature, are susceptible to localized surface damage/cracking when subjected to impact by foreign objects. It is also true that ceramic components may fail structurally even by soft particles when the kinetic energy of impacting objects exceeds certain limits. The latter case often has been found in aerospace engines in which combustion products, metallic particles or small foreign objects cause severe damage to blade/vane components, resulting in serious structural problems. Therefore, foreign object damage associated with particle impact needs to be considered when ceramic materials are designed for structural applications. In view of this importance, a considerable amount of work on impact damage of brittle materials by sharp particles as well as by “blunt” particles or by plates has been accumulated both experimentally and analytically [1–10]. The understanding of particle impact phenomena has been based on the concept of indentation fracture mechanics for sharp particle impact [2] and on Hertzian contact analysis for “blunt” or ball impact [1], leading to simplified quasi-static phenomenological models of strength degradation.

This paper describes in detail the ambient-temperature, foreign object damage (FOD) behavior of two currently representative gas-turbine grade silicon nitrides, AS800 and SN282. Some of the results in this work were also reported previously [11]. Ceramic target specimens in the form of flexure bars were impacted at their centers with *steel ball projectiles* with a diameter of 1.59 mm in a velocity range from 220 to 440 m/s. Post-impact strength was determined as a function of impact velocity to accurately evaluate the severity of impact damage. Fractography was performed before and after post-impact strength testing to determine impact morphologies and the nature of strength-controlling flaw configurations. A previously-proposed phenomenological model [1] was used to better understand the distinct difference in FOD behavior between the two silicon nitrides. To gain further insight, impact and post-impact strength testing was also conducted using an additional, equiaxed, fine-grained silicon nitride, NC132. Data obtained using this third silicon nitride material was utilized to further pinpoint a key material parameter affecting the FOD resistance of structural silicon nitrides.

*NASA Senior Resident Research Scientist at Glenn Research Center.

EXPERIMENTAL PROCEDURES

Materials and Test Specimens

Materials used in this work included two commercially available gas-pressure sintered silicon nitrides, AS800 (fabricated by Honeywell Engines, Phoenix, AZ, '99 vintage) and SN282 (fabricated by Kyocera, Vancouver, WA, '00 vintage). These two silicon nitrides are currently considered strong candidate materials for gas-turbine applications in view of their substantially improved elevated-temperature properties [12–14]. Both materials are toughened silicon nitrides, with microstructures tailored to achieve elongated grain structures. AS800 silicon nitride has been used at the NASA Glenn Research Center in life prediction programs [15,16]. The billets for each material were machined into flexure test specimens measuring 3 mm by 4 mm by 45 mm, respectively, in depth, width and length in accordance with a test standard ASTM C1161 (size “B”) [17]. All AS800 test specimens were annealed prior to testing at 1200 °C in air for 2h to eliminate or minimize damage and/or residual stresses presumably associated with machining. All SN282 test specimens were annealed by the manufacturer prior to testing with proprietary annealing condition.

A conventional, hot-pressed, equiaxed, fine-grained silicon nitride, NC132 (fabricated by Norton Advanced Ceramics, Northboro, MA, '90 vintage) [15], was also used for comparison. The dimensions and machining condition of flexure test specimens of NC132 silicon nitride were the same as those of AS800 and SN282. Test specimens were all annealed with the same annealing conditions applied to AS800.

The basic mechanical and physical properties of the three silicon nitrides as well as of the steel-ball projectile material (SAE 52100 bearing steel) are shown in Table 1.

Foreign Object Damage Testing

Foreign object damage (FOD) testing was carried out at ambient temperature using the experimental apparatus shown in Figure 1. A detailed description of the apparatus can be found elsewhere [11]. Hardened ($H_R C \geq 60$) chrome steel-balls with a diameter of 1.59 mm were inserted into a 300 mm-long gun barrel with an inner diameter of 1.59 mm. A He-gas cylinder and relief valves were used to pressurize the reservoir to a specific level depending on the prescribed impact velocity. Upon reaching a specific level of pressure, a solenoid valve was instantaneously opened accelerating a steel-ball projectile through the gun barrel to impact a target specimen that was *firmly* supported on a metallic specimen holder. Each target specimen was aligned such that the projectile impacted at the center (4 mm-wide side) of the test specimen with a normal incidence angle.

For a given pressure, the velocity of each steel projectile was determined using two pairs of laser transmitter and receiver, in which the two transmitters were aimed at the respective receivers through two holes in the gun barrel. The distance between the two holes was 25 mm, with the front hole located about 70 mm away from the front end of the gun barrel. The time traveled by a projectile between the two holes was measured with a digital storage oscilloscope connected to the two pairs of laser transmitter and receiver. The velocity was then calculated based on the distance-time relationship. It was found that velocity increased with increasing pressure, rising sharply at lower pressure but moderately at higher pressure as shown in Figure 2.

The range of impact velocity applied in this work was from 220 to 440 m/s. Typically 7 to 15 test specimens were impacted at each chosen velocity for a given material. In particular, to determine the statistical post-impact strength behavior of AS800 and SN282, a total of 15 to 17 test specimens were tested at an impact velocity of 300 m/s. Impact morphologies were selectively examined optically right after impact testing but prior to post-impact strength testing.

Table 1. Basic mechanical and physical properties of AS800, SN282 and NC132 silicon nitrides and steel-ball projectile material at ambient temperature

Material	Elastic modulus ¹ E (GPa)	Poisson's ratio ¹ ν	Density ² ρ (g/cm ³)	Hardness ³ H (GPa)
AS800 Si ₃ N ₄	309	0.27	3.27	13.6±1.4
SN282 Si ₃ N ₄	304	0.28	3.32	15.3±0.2
NC132 Si ₃ N ₄ [15]	315	0.30	3.20	14.0±0.2
Chrome steel (for ball projectiles) (SAE 52100)	200*	0.30*	7.80*	H _R C≥60*

Notes:

1. By the impulse excitation technique, ASTM C 1259 [18]
 2. By mass/volume method
 3. By Vickers microhardness indentation, ASTM C 1327 [19]
- * From the manufacturer's data; H_RC=Hardness in Rockwell C scale.

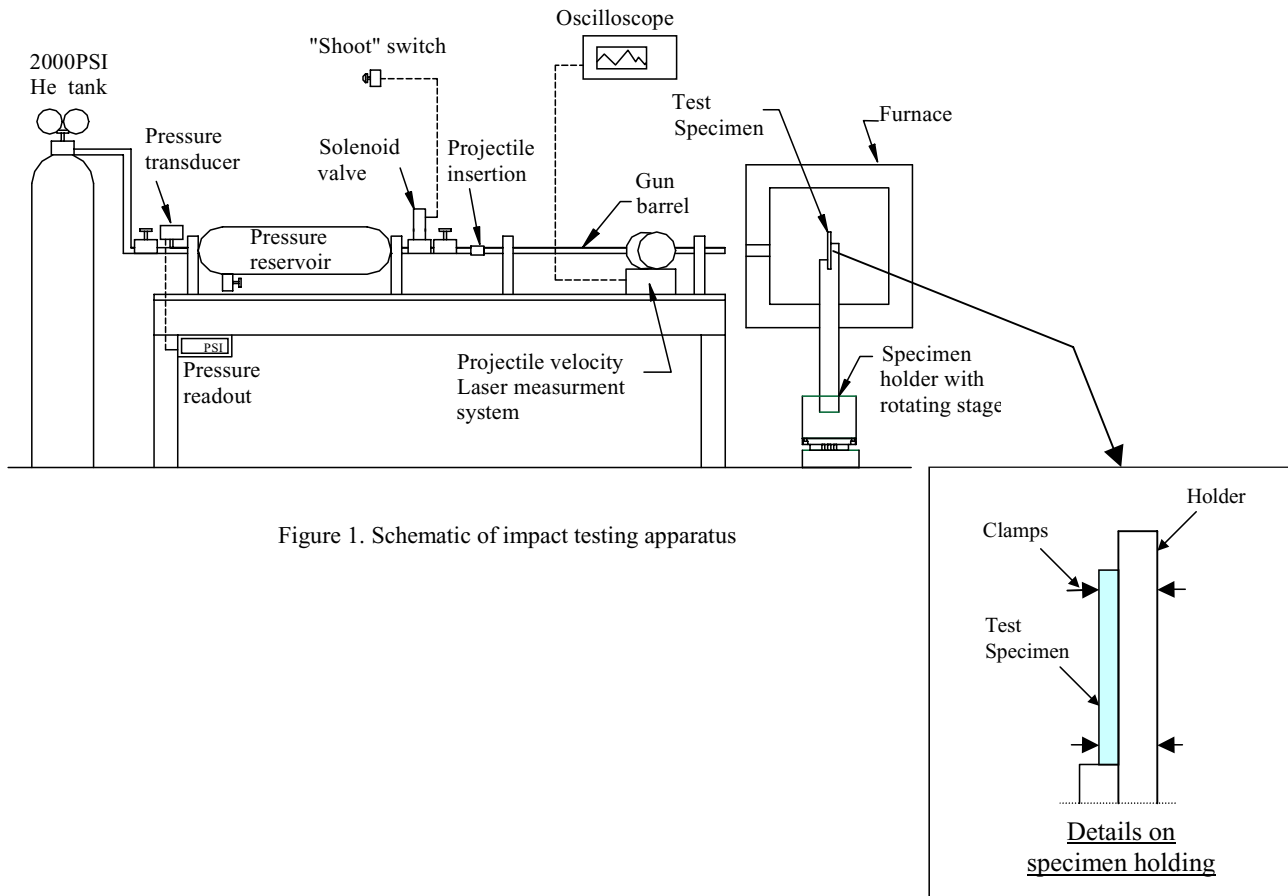


Figure 1. Schematic of impact testing apparatus

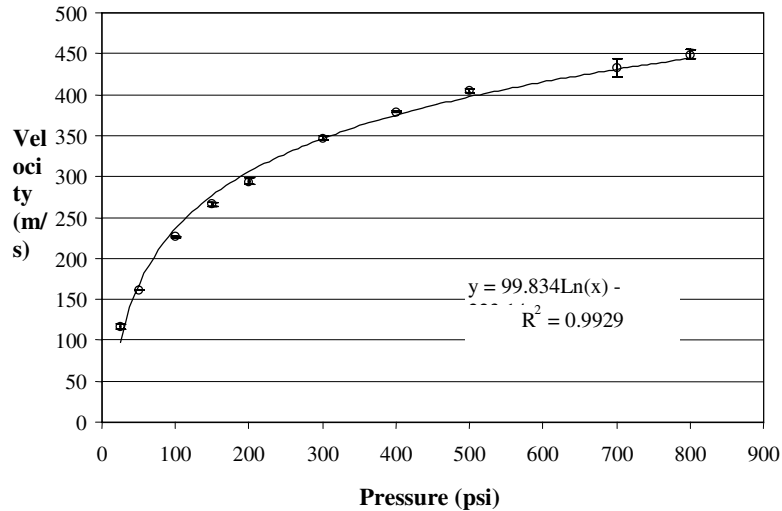


Figure 2. Velocity of steel ball projectiles with a diameter of 1.59 mm, as a function of He-pressure applied inside a gun barrel. Each data point represents an average of four measurements with an error bar of ± 1.0 standard deviation.

Post-Impact Strength Testing

Strength testing for impacted specimens was performed in ambient-temperature air using a SiC four-point flexure fixture with 20-mm inner and 40-mm outer spans in accordance with ASTM C 1161 [17]. Each impact-tested specimen was placed in the fixture such that its impact site was located in tension side within the inner span. An electromechanical test frame (Model 8562, Instron, Canton, MA) was used in displacement control with an actuator speed of 0.5 mm/min. Slow crack growth, which can occur during strength testing in air at ambient temperature for some ceramics such as alumina, is not an issue for silicon nitrides as well as silicon carbides. A limited fractographic analysis was performed after strength testing to determine failure origin, flaw configuration and mode of fracture. ‘As-received’ flexural strength was also determined for each material with a total of 20 test specimens using the same test fixture, test frame, and test conditions that were utilized for the impacted test specimens.

Fracture Toughness and Indentation Strength Testing

Fracture toughness was determined at ambient temperature for AS800 and SN282 using the single-edge-precracked beam (SEPB) method in accordance with ASTM C 1421 [20]. A total of five flexure test specimens with nominal dimensions of 3 mm (width) by 4 mm (depth) mm by 45 mm (length) were used for each material. A sharp precrack was introduced on the 3mm x 4mm plane located at the center of each test specimen. The average size of precracks, produced through Vickers indentation (with an indentation load of 9.8N) and subsequent bridge compression, was about 2 mm for both materials. Precracked specimens were fractured to determine fracture loads using a four-point flexure test fixture with 20-mm inner and 40-mm outer spans at 0.5 mm/min in an electromechanical test frame. Details regarding the SEPB test method in terms of relationship between indent load, bridge spans, and precrack size can be found elsewhere [21].

Indentation strength testing was also conducted using flexure test specimens measuring 3 mm (depth) by 4 mm (width) by 23 mm (length) in order to determine the material’s strength response to indentation damage by a Vickers indenter. This indentation-strength response has been used to model the quasi-static, sharp-particle impact behavior of brittle materials [2,3]. Hence, the use of indentation strength may enable one to at least qualitatively grasp an important material parameter that has the most significant effect on resistance to *sharp-particle* impact damage. Note that indentation strength data can also be used to determine R-curve behavior of brittle materials [22] in conjunction with fracture toughness data obtained by the SEPB method. Four different indentation loads of 29, 49, 98 and 196 N were applied on the 4-mm wide side at the center of each AS800 and SN282 test specimen. Indentation strength was determined using a four-point flexure fixture with 10-mm inner and 20-mm outer spans at a test rate of 0.5 mm/min with three test specimens tested at each indentation load. The number of test specimens, three at each

indentation load, was statistically sufficient considering a very small strength scatter (typically yielding a coefficient of variation of $\leq 5\%$) for both AS800 and SN282 silicon nitrides.

RESULTS AND DISCUSSION

Post-Impact Strength

The two-parameter Weibull plots of ‘as-received’ flexure strengths of both AS800 and SN282 are shown in Figure 3, where $\ln \ln[1/(1-F)]$ was plotted as a function of $\ln \sigma_f$. The variables F and σ_f are failure probability and flexure strength, respectively. Weibull modulus (m) and characteristic strength (σ_θ) were $m=21$ and $\sigma_\theta=795$ MPa for AS800, and $m=11$ and $\sigma_\theta=623$ MPa for SN282, respectively. The mean strength was 775 ± 45 MPa for AS800 and 595 ± 64 MPa for SN282. In many cases failure origins were associated with surface-connected defects such as machining flaws and pores, and with elongated grains.

The results of strength testing for impacted test specimens are shown in Figure 4, where post-impact strength was plotted as a function of impact velocity for both materials. ‘As-received’ flexure strength of both silicon nitrides was also plotted for comparison. Frequently, specimens impacted at lower velocity were not fractured from impact sites and were not included in the post-impact strength data. The ‘zero’ strength shown in the figure represents the specimens broken upon impact at higher velocity, where the impact force (or impact energy) was sufficient to break test specimens into two pieces, with failure originating from the impact site. This velocity is called a ‘critical impact velocity’ in this paper. It should be noted that for a given impact condition and material the critical impact velocity depends on test specimen size and geometry, as well as on the relative configuration of specimen support on impact test fixtures.

Strength degradation with respect to the ‘as-received’ strength was evident with increasing impact velocity for both materials. For a given impact velocity, however, corresponding post-impact strength was greater for AS800 than for SN282. Also, AS800 silicon nitride exhibited a higher critical impact velocity (V_c) as compared to that of SN282 silicon nitride such that

$$V_c \approx 400 \text{ m/s for AS800}$$

$$V_c \approx 300 \text{ m/s for SN282}$$

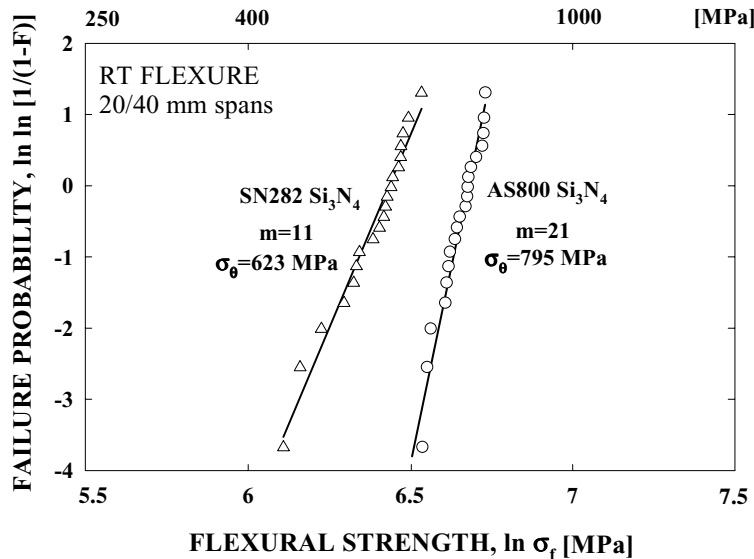


Figure 3. Weibull distributions of ‘as-received’ flexure strengths of AS800 and SN282 silicon nitrides determined at ambient temperature (‘RT’). m and σ_θ indicate Weibull modulus and characteristic strength, respectively. The straight lines represent best-fit lines.

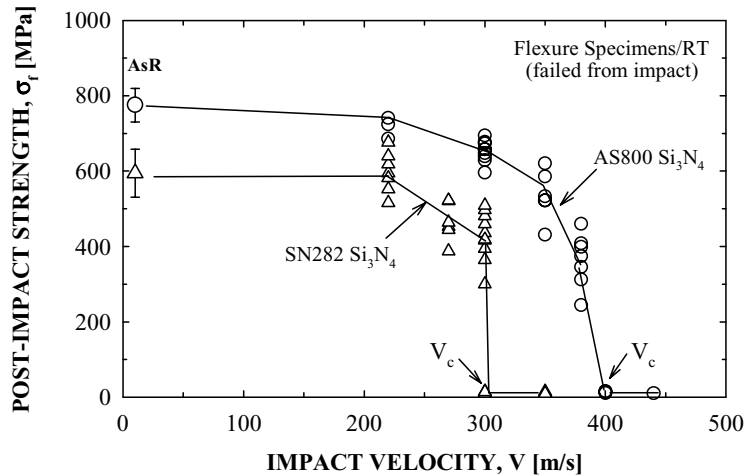


Figure 4. Results of post-impact strength as a function of impact velocity, determined for AS800 and SN282 silicon nitrides flexure specimens impacted at ambient temperature (“RT”) by steel ball projectiles with a diameter of 1.59mm. “AsR” indicates ‘as-received’ mean flexure strength of two materials with error bars of ± 1.0 standard deviations. V_c (with arrows) indicates the “critical impact velocity.”

Sharp strength degradation occurred in the region of impact velocities close to the critical impact velocity of each material. The post-impact strength behavior of both materials was better represented in a two-parameter Weibull scheme, which is depicted in Figure 5. The figure is for a given impact velocity of 300 m/s using a somewhat large number (15 to 17) of test specimens. For AS800 silicon nitride, nine of a total 17 test specimens failed from impact sites and the remaining eight specimens failed from inherent material defects, resulting in a uni-modal strength distribution (with a Weibull modulus of about 20, close to that of the as-received strength). By contrast, for SN282 silicon nitride, all 15 test specimens fractured from impact sites; however, five of these 15 specimens broke upon impact, thereby resulting in an overall bimodal strength distribution. Note that the (“zero”) strength for the specimens that failed upon impact for SN282 was taken to be about 10 MPa for graphical presentation.

Impact Morphology

The hardened steel ball projectiles, without exception, were flattened after impact, as a result of considerable plastic deformation. In some cases, particularly at higher impact velocity, the projectiles were subjected to both extreme heat (evidenced by burning marks) and cracking, as shown in Figure 6. The degree of plastic deformation of the projectiles in terms of projectile-diameter decrease was about 20 to 40% depending on velocity. The mechanical properties of a projectile material, of course, are important factors affecting FOD behavior of a target material. A preliminary study showed that annealed steel ball projectiles were more susceptible to plastic deformation than the hardened steel ball projectiles, and thus caused less damage to the target material.

Impact sites were characterized with three distinct regions of inner, intermediate and outer zones, see Figure 7. The inner zone was typically on the top of cone cracks, the intermediate zone was believed to be the outer boundary of lateral cracks or other damage, and the outer zone was of the impression of flattened steel-ball projectiles. Some material transfer from the projectiles to the target specimens was seen at the outer zone, due to an instantaneous ‘cold welding’ effect (by metallic projectiles) at the contact area. In post-impact strength testing, failure of specimens impacted at velocities below critical impact velocity commonly originated from the outer boundary of lateral cracks (see Figure 7(b)). The failure path in this case was straight and cut through the boundary of the intermediate damage zone. Well-developed cone cracks were observed in specimens impacted at velocity close to and above the “critical impact velocity” in which test specimens fractured into two pieces upon impact. The surface failure pattern associated with this well-developed cone crack was clearly typified with a fracture path that was kinked at the inner damage zone that was an upper part of the cone (Figure 7(c)).

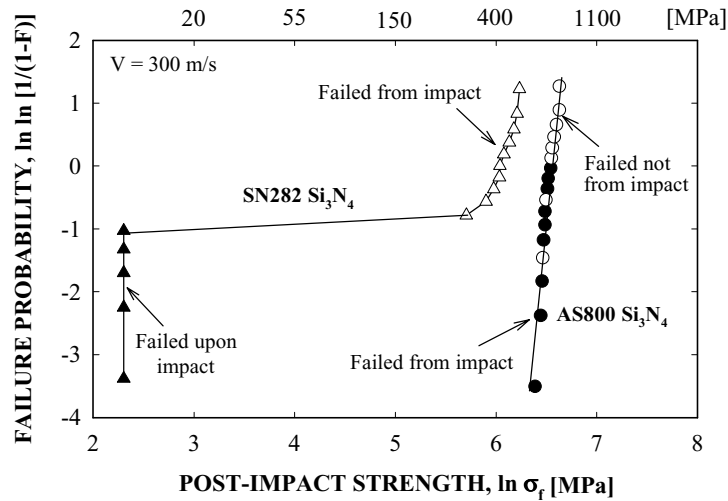


Figure 5. Weibull strength distributions for AS800 and SN282 silicon nitrides flexure specimens impacted at 300 m/s by 1.59-mm-diameter steel ball projectiles. The strength for the SN282 specimens completely fractured upon impact was taken to be about 10 MPa for presentation purpose. The open symbols for AS800 indicate the specimens not failed from impact sites, whereas the closed symbols represent the specimens failed from impact sites.

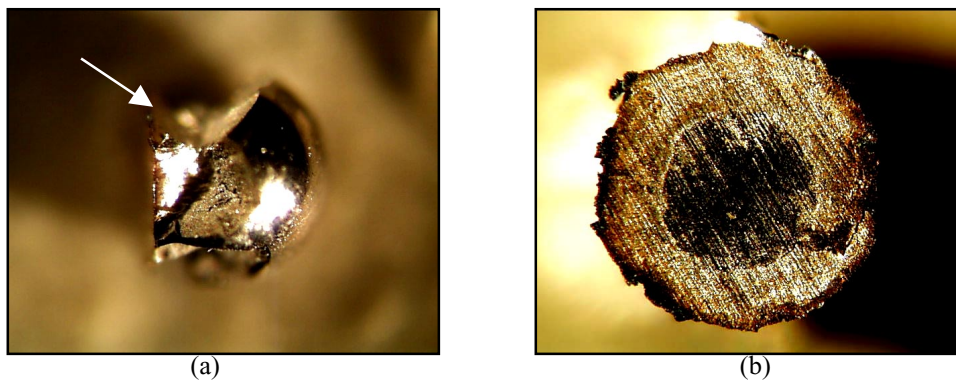


Figure 6. A typical example of a steel ball projectile with a diameter of 1.59 mm subjected to an impact velocity of 350 m/s for AS800 silicon nitride, showing severe plastic deformation (flattened), heating and cracking: (a) side view; (b) top view from the arrow. Note the impression marks in (b), imprinted from the machining marks of an AS800 target specimen.

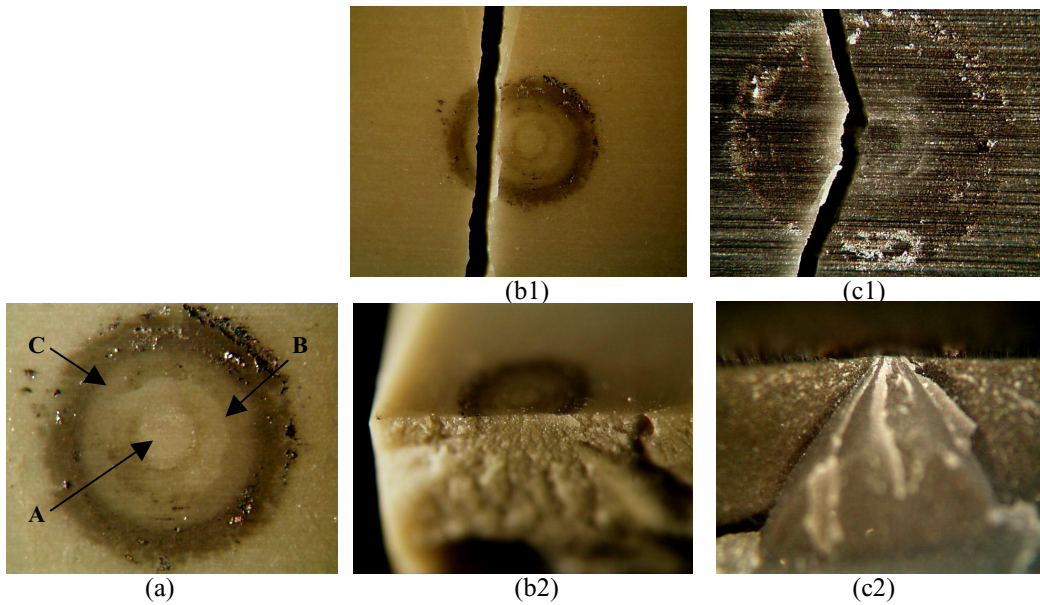


Figure 7. Typical examples of the impact sites, fracture surfaces and fracture paths for both AS800 and SN282 silicon nitrides subjected to steel ball projectiles with a diameter of 1.59 mm: (a) Overall impact site showing three distinct regions (“A”: inner zone, “B”: intermediate zone and “C”: outer zone) for AS800 at an impact velocity of $V=350$ m/s; (b) Top fracture path (b1) and fracture surface (b2) of an AS800 specimen failed (in strength testing) from the outer boundary of the intermediate damage zone; strength = 650 MPa; (c) A SN282 specimen failed upon impact at $V=350$ m/s showing kinked fracture path (c1) at the cone and fracture surface (c2) showing a well-developed cone crack.

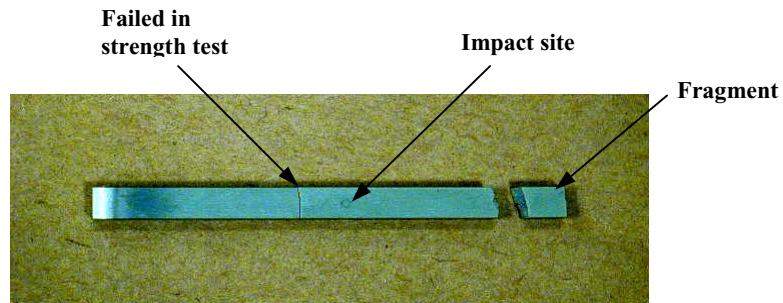


Figure 8. An AS800 test specimen broken at a distance of about 5 mm from the right end upon impact at a velocity of 300 m/s. The impact site is visible. The specimen was strength-tested, but failure did not originate from the impact site.

The tensile principal stress, according to the Hertzian contact analysis, occurs just outside the contact area between two contacting bodies in which a cone crack initiates and then propagates through the locus of maximum tensile stress [5,9]. In cases of impacts with hard projectiles vs. hard target materials (such as ceramic balls vs. ceramic target materials), reasonable agreement between the calculated contact area (radius) and the upper size (radius) of a cone has been demonstrated [4]. The contact area can be estimated based on the Hertzian contact theory together with the principle of conservation of impact energy as follows [1,4,5,8]:

$$a = \alpha(k/E)^{1/5} \rho^{1/5} R V^{2/5} \quad (1)$$

where a is the contact area, α is a constant (≈ 1.3), $k = [(1-\nu^2)+(1-\nu'^2)E/E']$ with ν being Poisson's ratio and the primes denoting variables associated with the projectile, E is the elastic modulus of target material, ρ is the density of the projectile, R is the radius of the projectile, and V is the impact velocity. The calculated contact area based on Equation (1) was significantly smaller (approximately one-fifth) than the upper cone sizes observed in the current effort. Significant plastic deformation of steel ball projectiles is believed to be a major cause of such a discrepancy between the calculated and the observed contact size. Evidently the 'soft' steel balls generated much less contact area compared to that generated with 'hard' ceramic balls. Hence, the impact events in this work would be characterized as 'plastic (in projectile)-elastic (in target material)' impact rather than 'elastic-elastic' impact, which would be the case for ceramic balls vs. ceramic target. Of course, plastic deformation may possibly occur even in *ceramic* projectiles and target materials upon Hertzian impact. In the current effort, any plastic deformation potentially occurring in the ceramic target materials was assumed negligible as compared with the degree of plastic deformation of the *steel* ball projectiles.

Finally it was found that in some rare cases (particularly at 300 m/s) some specimens failed upon impact at a distance of about 5–8 mm from one end of the test specimen, as shown in Figure 8. This is presumably a result of stress wave interaction (dynamic effect) upon impact, similar in principle to the situation of Hopkinson bar experiments. Although this was observed as a rare case in the current experimental setting, such dynamic effects must be considered in instances where real components are subjected to high impact energy.

Fracture Toughness, Indentation Strength and R-Curve

A summary of fracture toughness for AS800 and SN282 silicon nitrides determined by the SEPB method is shown in Table 2. The table also includes the value previously evaluated for the conventional fine-grained NC132 silicon nitride [15]. Fracture toughness was $K_{IC} = 8.1 \pm 0.3$ MPa \sqrt{m} and $K_{IC} = 5.5 \pm 0.2$ MPa \sqrt{m} , respectively, for AS800 and SN282 silicon nitrides. Both AS800 and SN282 silicon nitrides are known as *in-situ* toughened materials tailored to achieve elongated grain structures. Consequently, the tailored microstructure of these materials results in increased fracture toughness, as compared to conventional equiaxed, fine-grained silicon nitrides.

Table 2. Fracture toughness of AS800, SN282 and NC132 silicon nitrides determined in four-point flexure at ambient temperature

Material	No. of test specimens	Fracture toughness, K_{IC} (MPa \sqrt{m})	Method [20]
AS800 Si ₃ N ₄	5	8.1 \pm 0.3	SEPB
SN282 Si ₃ N ₄	5	5.5 \pm 0.2	SEPB
NC132 Si ₃ N ₄ [15]	5	4.6 \pm 0.4	SEPB

Indent strength as a function of indent load determined for both silicon nitrides (AS800 and SN282) is shown in Figure 9. For a given indent load, indent strength was greater for AS800 than for SN282. Based on indentation fracture mechanics, generalized indent strength (σ_{if}) can be expressed as a function of indent load (P) as follows [22]:

$$\sigma_{if} = \phi P^{\frac{2\beta-1}{3+2\beta}} \quad (2)$$

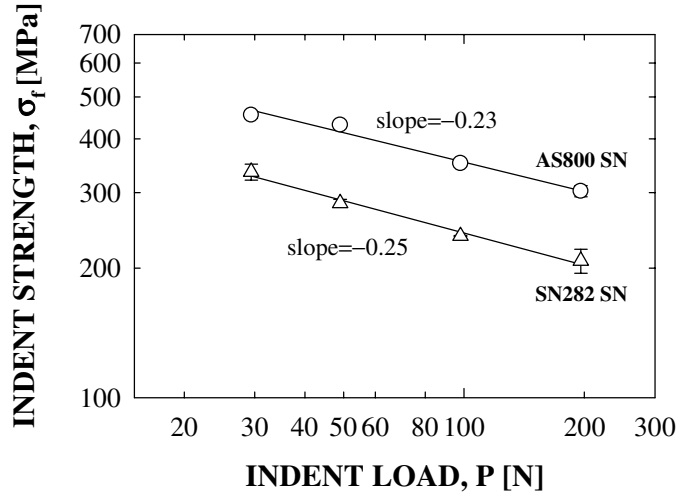


Figure 9. Indent strength as a function of indent load determined for AS800 and SN282 silicon nitrides. The solid lines represent the best-fit lines in the log (*indent strength*) vs. log (*indent load*) relation. Error bars indicate ± 1.0 standard deviations.

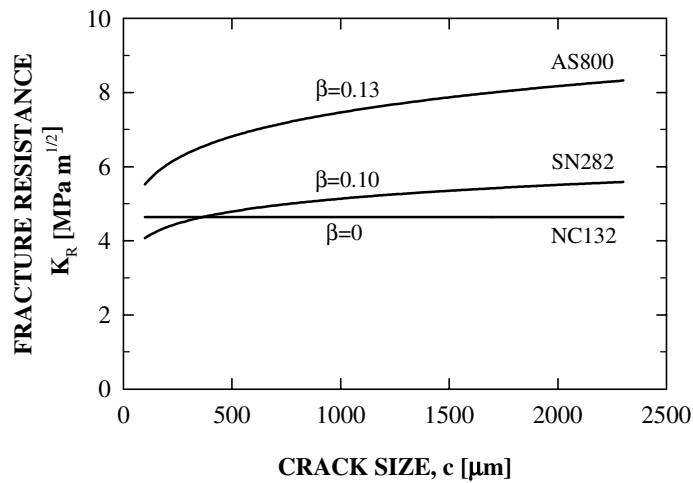


Figure 10. Fracture resistance (R-curve) as a function of crack size for AS800 and SN282 silicon nitrides. The fine-grained NC132 silicon nitride data [15] is also included for comparison.

where ϕ is a parameter associated with elastic modulus, hardness, indent crack geometry and fracture resistance. The parameter β represents the degree of fracture resistance (“R-curve”) as defined in [22]

$$K_R = \kappa c^\beta \quad (3)$$

where K_R is fracture resistance, c is the crack size, and κ is a parameter. Equation 2 is a common expression of rising R-curve behavior for ceramic materials. When $\beta=0$, the case reduces to a flat R-curve such that $\sigma_{ij}=\phi P^{-1/3}$ and $K_R=\kappa=K_{IC}$. R-curve behavior of a brittle material can be estimated based on Equation (3) by determining the parameter β from (the slope of) the indent strength vs. indent load data (such as Figure 9) and then using this value to determine the parameter κ using a known value of fracture toughness (obtained by, for example, SEPB) evaluated with the particular precrack size (c) used. The resulting R-curve behavior thus estimated for AS800 and SN282 is shown in Figure 10. The previously determined R-curve of NC132 silicon nitride [15] is also included in the figure. AS800 exhibits not only greater fracture toughness but also stronger R-curve behavior than SN282, while the conventional, equiaxed fine-grained NC132 silicon nitride typically exhibits a flat R-curve and low fracture toughness.

Analytical Considerations on Strength Degradation

A phenomenological model of strength degradation due to *ball impact* was proposed previously by Wiederhorn and Lawn [1], based on assumptions that the impact event was elastic and quasi-static and that strength degradation was attributed to a formation of cone cracks. Also, another important assumption was that the “effective” size of strength controlling flaws was proportional to the base radius of the cone [1,5,9]. The latter simplification was based on the fact that the stress intensity factor solution of a cone crack was not available and that the geometry of a cone crack system varied with projectile, target materials and impact conditions (velocity), etc. With those assumptions, strength degradation was modeled using Hertzian contact analysis, the principle of energy conservation, and indentation fracture relations. The model, despite several assumptions, was in good agreement with experimental data determined for glass impacted by steel or tungsten carbide spherical projectiles [1]. The resulting strength degradation as a function of impact velocity is expressed as follows [1]:

$$\sigma_f = \Phi(k/E)^{2/15} \rho^{-1/5} R^{-2/3} K_{IC}^{4/3} V^{-2/5} \quad (4)$$

where Φ is a constant. Equation (4) can also be expressed in terms of impact kinetic energy (U_K) of a projectile using

$$U_K = \frac{1}{2} m V^2 \quad (5)$$

to yield

$$\sigma_f = \Phi'(k/E)^{2/15} R^{-1/15} K_{IC}^{4/3} U_K^{-1/5} \quad (6)$$

where m is the mass of a projectile and $\Phi'=(2\pi/3)^{1/5} \Phi$. For a given target material and a given material and geometry of a projectile, the post-impact strength depends on [impact velocity]^{-2/5} or [impact kinetic energy]^{-1/5} as seen from Equation (4) or (6). The post-impact strength data shown in Figure 4 were plotted as a function of impact kinetic energy in Figure 11 based on Equation (6). It is noted from the figure that a discrepancy in slope between the prediction (=−1/5) and the experimental data was significant for both AS800 and SN282 silicon nitrides. This discrepancy might have arisen from several factors, including: (1) Significant plastic deformation of a projectile upon impact might invalidate the model’s assumption of idealized elastic impact;

(2) Formation of well-developed cone cracks might not have always occurred (as seen from fractography); sometimes radial or lateral cracks or ill-defined damage might have controlled

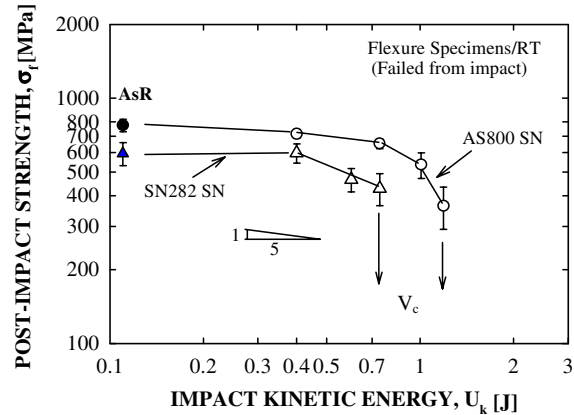


Figure 11. Post-impact strength as a function of impact kinetic energy determined for AS800 and SN282 silicon nitrides. The slope ($=-1/5$) indicates a theoretical value based on Equation (4). “AsR” indicates “as-received” flexure strength for both materials. For clarity of graphical representation, mean strength was used with error bars of ± 1.0 standard deviations.

strength; (3) Quasi-static assumption of the model, which would have been operative for *soft* glasses, might not have been applicable to harder silicon nitrides.

A Key Material Parameter Affecting FOD Resistance

For most silicon nitrides, elastic modulus (E), hardness, density and Poisson’s ratio (ν) are quite similar. Hence for a given projectile, impact velocity, and given target specimen geometry, the post-impact strength, according to Equation (4) or (6), depends on the fracture toughness of a target material with a relation of $\sigma_f \propto [K_{IC}]^{4/3}$. This leads to a simple expression of the post-impact strength ratio between AS800 and SN282 silicon nitrides as follows:

$$\frac{\sigma_{f/AS800}}{\sigma_{f/SN282}} = \left[\frac{K_{IC/AS800}}{K_{IC/SN282}} \right]^{4/3} \tag{7}$$

Use of this relation together with the values of fracture toughness (see Table 2) determined for both AS800 and SN282 yielded that the post-impact strength of AS800 was 1.68 times greater than that of SN282. The actual strength ratio at 200 m/s and 300 m/s was found to be 1.20 and 1.52, respectively, resulting in reasonable agreement, particularly at 300 m/s. Despite an appreciable discrepancy in the post-impact strength vs. impact kinetic energy relation between the prediction and the experimental data, as seen in Figure 11, Equation (4) or (6) provides important insight regarding AS800’s greater resistance to FOD as compared to that of SN282. It is therefore reasonable to conclude that a silicon nitride with greater fracture toughness can possess greater FOD resistance than another silicon nitride with lower fracture toughness.

In order to better understand (and thus to further confirm) this major conclusion, additional FOD testing was conducted using a conventional, equiaxed, fine-grained silicon nitride (NC132) for target/strength test specimens, as described previously in the Experimental Procedure. The results of post-impact strength testing for NC132 silicon nitride are presented in Figure 12,

*This relation, based on indentation fracture mechanics [23], is valid for indent strength for a given indent load. The ratio of indent strength between AS800 and SN282 silicon nitrides shown in Figure 9 was in the range of 1.36 to 1.52, resulting in some discrepancy with the theoretical prediction ($=1.68$) but overall in reasonable agreement.

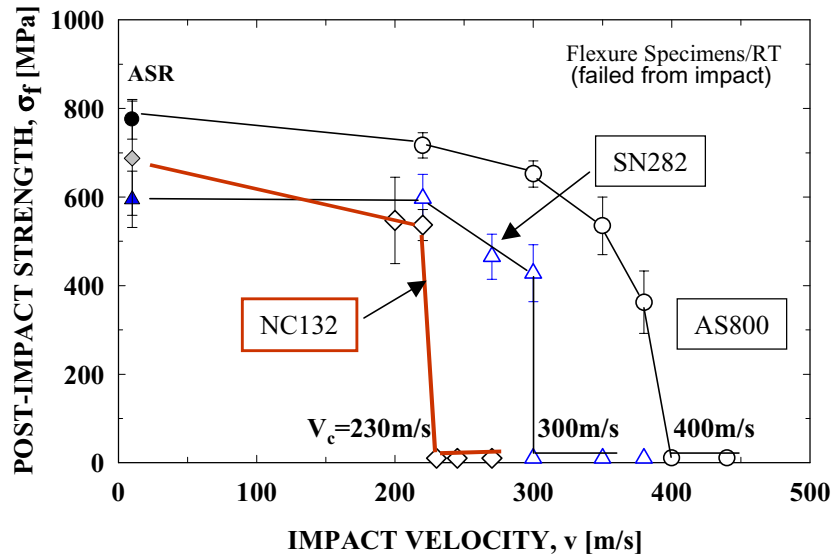


Figure 12. Results of post-impact strength as a function of impact velocity for NC132 silicon nitride, presented together with AS800 and SN282 silicon nitride data for comparison. Mean strength was used for graphical clarity with error bars of ± 1.0 standard deviations. V_c indicates critical impact velocity.

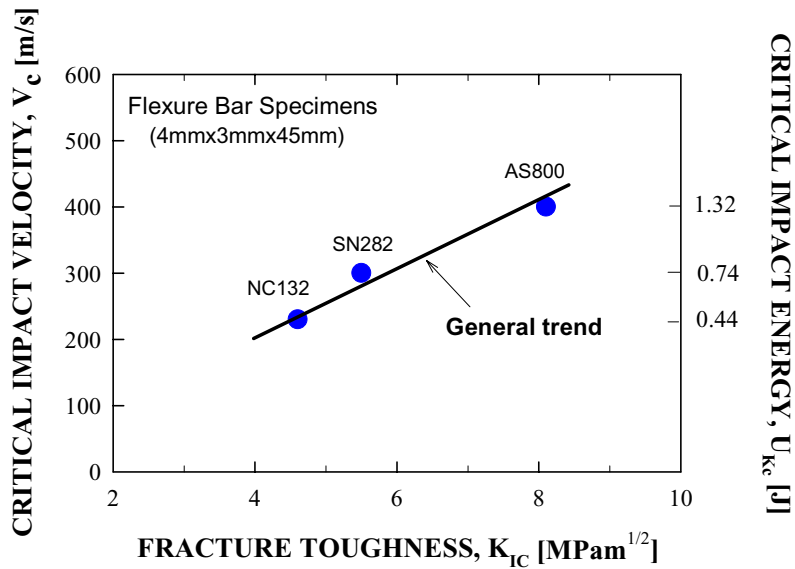


Figure 13. General trend in critical impact velocity as a function of fracture toughness for two in-situ toughened AS800 and SN282 silicon nitrides and one conventional, equiaxed fine-grained NC132 silicon nitride.

degradation of NC132 with respect to “as-received” strength was significant even at lower impact velocities (≤ 220 m/s), resulting in the lowest critical impact velocity of $V_c=230$ m/s among the three silicon nitrides tested. Figure 13 shows a summary of critical impact velocity as a function of fracture toughness for the three silicon nitrides tested. The general trend manifest from the figure is that critical impact velocity increases with increasing fracture toughness. This indicates undoubtedly that fracture toughness is a key material parameter affecting FOD resistance in silicon nitrides. This is also understandable if one considers that fracture toughness is a measure of resistance to crack initiation-and-propagation. The NC132 with the lowest value of fracture toughness, $K_{IC}=4.6$ MPa \sqrt{m} , exhibited the lowest FOD resistance; whereas, the AS800 with the greatest value of fracture toughness, $K_{IC}=8.1$ MPa \sqrt{m} , showed the greatest FOD resistance. In other words, the in-situ toughened silicon nitride, tailored with an elongated grain structure to achieve more fracture resistance (and rising R-curve behavior also) via crack deflection and/or bridging, additionally possesses much better FOD resistance than the conventional, equiaxed, fine-grained silicon nitride which has no such features as deflection and/or bridging, and typically exhibits a flat R-curve (see Figure 10).

Comparison of FOD Behavior between ‘Blunt’ (Ball) Projectile and Sharp-Particle Impact

A comparison of post-impact strength of silicon nitrides subjected to a single impact event with steel balls (this study) and sharp SiC-particles (grit # 16 and 46) [3,24] is shown in Figure 14. Considerable strength degradation occurs in the case of sharp particle impact even at much lower impact kinetic energy, showing that the severity of impact damage was far greater in “sharp” particle impact than in “blunt” (steel-ball) projectile impact. The sharp particle impact typically produced radial cracks emanating from the impact sites (similar to the Vickers indent cracks that originate from the corners of an impression site), thereby resulting in significant strength degradation. It should be noted that the fracture toughness of AS440 silicon nitride was greater (about 30%) than that of GN10 silicon nitride; hence, as expected, the post-impact strength observed for sharp particle impact was greater for AS440 than for GN10. Figure 15 shows typical morphologies generated by three different types of damages: steel-ball projectile impact (this study), sharp SiC-particle impact [24], and Vickers indent [24]. Radial cracks, originating from the impact site and causing appreciable strength degradation, were typified in sharp-particle impact. Cone and lateral cracks, resulting in relatively insignificant strength degradation, were exemplified in steel-ball projectile impact. Well-developed radial/median crack systems are generally characterized in most silicon nitrides in response to Vickers indent. As a consequence, for a given (quasistatic) impact load, strength degradation is expected to be much greater in either sharp-particle impact or static indentation than in ball projectile impact. Of course, the degree of strength degradation for sharp particle impact also depends on additional features such as the geometry and material of particles and target specimens.

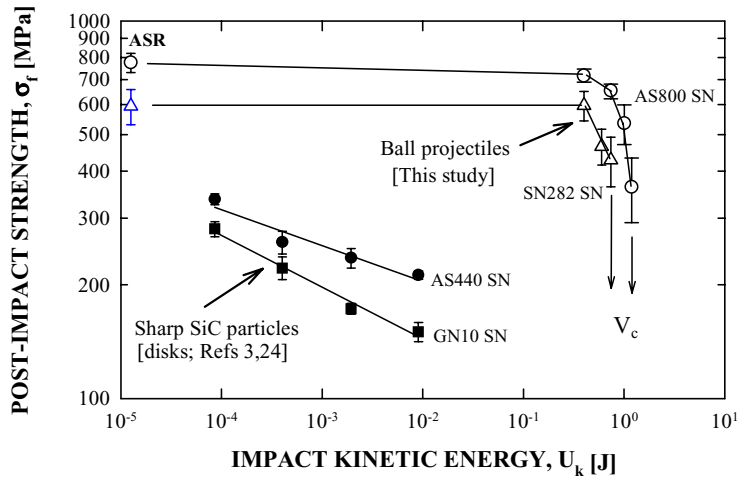


Figure 14. A comparison of post-impact strength as a function of impact kinetic energy between “sharp” SiC particle impact [3,24] and “blunt” steel-ball projectile impact (this study). “ASR” indicates “as-received” flexure strength for both materials. Error bars represent ± 1.0 standard deviations.

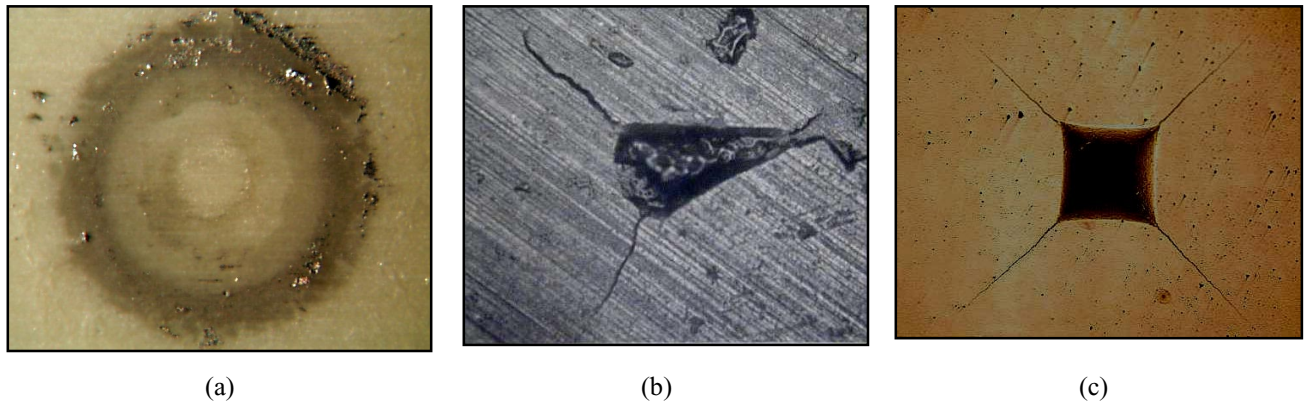


Figure 15. Three different types of damages generated in machined surfaces of silicon nitrides at ambient temperature by: (a) steel-ball projectile impact (this study), (b) sharp SiC-particle impact [24], and (c) a Vickers indenter [24].

Effect of Protective Layer: Role of Protective Coating

It is speculated that for a given projectile and target material, FOD resistance can be improved by employing a certain protective coating. Essentially, this coating would reduce the severity of impact damage by alleviating the magnitude of Hertzian contact stresses. With this in mind, additional FOD testing for both AS800 and SN282 silicon nitrides was conducted at impact velocities greater than the critical impact velocities for each of the two materials. The prospective impact site on each target specimen was covered with 0.059mm-thin copper shim (tape), i.e., a protective layer. Three specimens of each silicon nitride were tested, yielding the results shown in Figure 16. The average post-impact strength of AS800 with the protective layer at an impact velocity of 440 m/s was 580 MPa. The addition of a protective layer provided a remarkable enhancement in FOD resistance, compared to the AS800 specimens tested previously (with no protective layer) that resulted in ‘zero’ post-impact strength. The same effect was observed for SN282, where an average post-impact strength of 365 MPa was achieved with the protective layer at an impact velocity of 400 m/s, which is significantly greater than the critical impact velocity of 300 m/s observed previously in the case with no protective layer. This indicates that the thin copper shim did indeed act as a protective layer, reducing the severity of impact damage by reducing Hertzian contact stress. However, it should be noted that the protective layer just blew up upon impact, see Figure 17, thus making the layer ineffective against multiple or repeated impact events. These results indicate that the addition of a protective layer on the base silicon nitride increases the critical impact velocity significantly and that adhesion between the protective layer and the substrate is crucial to enhance the life of the protective layer. It is also implied that greater fracture toughness of a protective layer will yield better FOD resistance as well as increased life of the underlying silicon nitride material. Protective coatings have been an important issue in demanding aeroengine environments. Application of thermal barrier coatings (TBCs) and/or environmental barrier coatings (EBCs) has been shown to provide significant performance enhancements. In addition to TBC/EBC, the application of protective coatings to improve FOD resistance—‘impact barrier coating’ (IBC) or ‘impact resistance coating’ (IRC)—must be considered, explored, and developed as an important necessity in aeroengine design and applications.

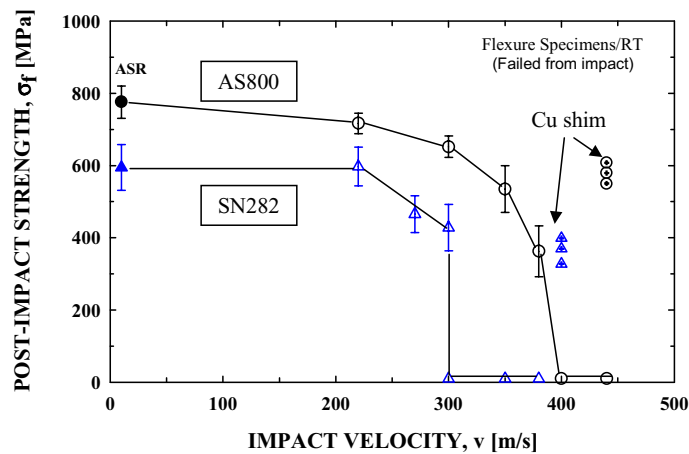


Figure 16. Results of impact testing for AS800 and SN282 silicon nitrides with test specimens being covered with 0.059-mm copper protective layer (shim). Impact velocity used was 400 and 440 m/s, respectively, for SN282 and AS800 silicon nitrides. The results of the regular (no protective coating) FOD tests are also shown for comparison.

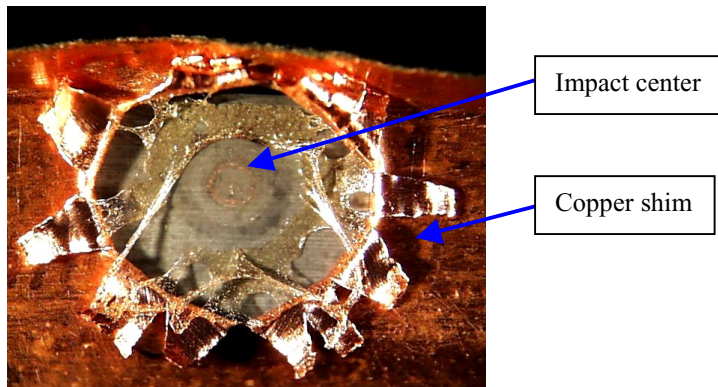


Figure 17. A typical appearance of the impact site of 0.059-mm thick copper shim and SN282 test specimen subjected to an impact velocity of 400 m/s. Note a blew-up mode of copper shim upon impact. The post-impact strength of this specimen was determined as 327 MPa.

Other Considerations

Designing aeroengine components to withstand FOD events is a complex task. Consideration of many factors is required, both in the generation of FOD data as well as in actual component design efforts. A sample of these numerous factors includes the following:

- Effect of projectile material/geometry
- Effect of test specimen material/geometry: monolithic vs. composites approach
- Effect of test-specimen support and component attachment
- Effect of temperature/environment
- Appropriate protective coatings
- Geometrical design of components to enhance FOD resistance
- FOD/Reliability/Life prediction codes

Not only must each of these factors be scrutinized individually, but the effects of interactions between multiple factors also must be accommodated. Notwithstanding the immense challenges this poses, a strategy for mitigating FOD damage must be developed and employed in order to achieve the most desirable performance of components in service. Hence, some of these factors are immediate subjects of study and the related work is under way, such as in the tasks reported in this manuscript. Others are long-term efforts and are pursued continually in the quest for improving the efficiency and reliability of aeroengine components.

CONCLUSIONS

Based on the results of extensive FOD testing at ambient temperature for two in-situ toughened, gas-turbine grade silicon nitrides (AS800 and SN282) and one conventional silicon nitride (NC132), the following conclusions were made:

- (1) The overall resistance—estimated by post-impact strength - to foreign object damage (FOD) by steel-ball projectiles with a diameter of 1.59 mm was found to be greater for AS800 silicon nitride than for SN282 silicon nitride in an impact velocity range of 220 to 440 m/s.

- (2) The critical impact velocity, in which flexure test specimens fractured upon impact, was about 400 m/s and 300 m/s, respectively, for AS800 and SN282 silicon nitrides. The critical impact velocity of the conventional equiaxed fine-grained NC132 silicon nitride was about 230 m/s.
- (3) The difference in FOD resistance between AS800 and SN282 silicon nitrides was found to be due to differences in fracture toughness, as also supported by additional FOD data on NC132 with low fracture toughness. The critical impact velocity, in general, was linearly dependent on fracture toughness, leading to a conclusion that fracture toughness is a *key material parameter* affecting FOD resistance of silicon nitrides.
- (4) The impact damage by ‘blunt’ steel-ball projectiles was found to be far more insignificant for a given impact kinetic energy than that by ‘sharp’ SiC particles.
- (5) The addition of a protective layer of 0.059-mm copper shim significantly improved the FOD resistance of both AS800 and SN282 silicon nitrides by considerably reducing the severity of impact damage via alleviating Hertzian contact stresses. This gives an insight into some practical design philosophy regarding FOD protective coatings in actual aeroengine components.

REFERENCES

1. S.M. Wiederhorn and B.R. Lawn, “Strength Degradation of Glass Resulting from Impact with Spheres,” *J. Am. Ceram. Soc.*, **60**[9–10] 451–458 (1977).
2. S.M. Wiederhorn and B.R. Lawn, “Strength Degradation of Glass Impact with Sharp Particles: I, Annealed Surfaces,” *J. Am. Ceram. Soc.*, **62**[1–2] 66–70 (1979).
3. J.E. Ritter, S.R. Choi, K. Jakus, P.J. Whalen, and R.G. Rateick, “Effect of Microstructure on the Erosion and Impact Damage of Sintered Silicon Nitride,” *J. Mater. Sci.*, **26** 5543–5546 (1991).
4. Y. Akimune, Y. Katano, and K. Matoba, “Spherical-Impact Damage and Strength Degradation in Silicon Nitrides for Automobile Turbocharger Rotors,” *J. Am. Ceram. Soc.*, **72**[8] 1422–1428 (1989).
5. C.G. Knight, M.V. Swain, and M.M. Chaudhri, “Impact of Small Steel Spheres on Glass Surfaces,” *J. Mater. Sci.*, **12** 1573–1586 (1977).
6. A.M. Rajendran and J.L. Kroupa, “Impact Design Model for Ceramic Materials,” *J. Appl. Phys.*, **66**[8] 3560–3565 (1989).
7. L.M. Taylor, E.P. Chen, and J.S. Kuszmaul, “Microcrack-Induced Damage Accumulation in Brittle Rock Under Dynamic Loading,” *Comp. Meth. Appl. Mech. Eng.*, **55**, 301–320 (1986).
8. R. Mougnot and D. Maugis, “Fracture Indentation beneath Flat and Spherical Punches,” *J. Mater. Sci.*, **20** 4354–4376 (1985).
9. A.G. Evans and T.R. Wilshaw, “Dynamic Solid Particle Damage in Brittle Materials: An Appraisal,” *J. Mater. Sci.*, **12** 97–116 (1977).
10. B.M. Liaw, A.S. Kobayashi, and A.G. Emery, “Theoretical Model of Impact Damage in Structural Ceramics,” *J. Am. Ceram. Soc.*, **67** 544–548 (1984).
11. S.R. Choi, J.M. Pereira, L.A. Janosik, and R.T. Bhatt, “Foreign Object Damage of Two Gas-Turbine Grade Silicon Nitrides at Ambient Temperature,” (in print) *Ceram. Eng. Sci. Proc.*, **23**[3,4] (2002).
12. T. Ohji, “Long Term Tensile Creep Behavior of Highly Heat-Resistant Silicon Nitride for Ceramic Gas Turbines,” *Ceram. Eng. Sci. Proc.*, **22**[3] 159–166 (2001).
13. F. Lofaj, S.M. Wiederhorn, and P.R. Jemian, “Tensile Creep in the Next Generation Silicon Nitride,” *Ceram. Eng. Sci. Proc.*, **22**[3] 167–174 (2001).
14. H.T. Lin, S.B. Waters, K.L. More, J. Wimmer, and C.W. Li, “Evaluation of Creep Property of AS800 Silicon Nitride from As-Processed Surface Regions,” *Ceram. Eng. Sci. Proc.*, **22**[3] 175–182 (2001).

15. S.R. Choi and J.P. Gyekenyesi, (a) "Elevated-Temperature "Ultra"-Fast Fracture Strength of Advanced Ceramics: An Approach to Elevated-Temperature "Inert" Strength," *ASME J. Eng. Gas Turbines & Powers*, **121** 18–24 (1999); (b) "'Ultra'-Fast Strength of Advanced Structural Ceramics at Elevated Temperatures" pp. 27–46 in *Fracture Mechanics of Ceramics*, Vol. 13, Edited by R.C. Bradt, D. Munz, M. Sakai, V.Ya. Shevchenko, and K.W. White, Kluwer Academic/Plenum Publishers, New York, NY (2002).
16. S.R. Choi and J.P. Gyekenyesi, "Slow Crack Growth Analysis of Advanced Structural Ceramics under Combined Loading Conditions: Damage Assessment in Life Prediction Testing," *ASME J. Eng. Gas Turbines & Power*, **123** 277–287 (2001).
17. ASTM C 1161, "Test Method for Flexural Strength of Advanced Ceramics at Ambient Temperatures," *Annual Book of ASTM Standards, Vol. 15.01*, ASTM, West Conshohocken, PA (2002).
18. ASTM C 1259, "Test Method for Dynamic Young's Modulus, Shear Modulus, and Poisson's Ratio for Advanced Ceramics by Impulse Excitation of Vibration," *Annual Book of ASTM Standards, Vol. 15.01*, ASTM, West Conshohocken, PA (2002).
19. ASTM C 1327, "Test method for Vickers Indentation Hardness of Advanced Ceramics," *Annual Book of ASTM Standards, Vol. 15.01*, ASTM, West Conshohocken, PA (2002).
20. ASTM C 1421, "Test Methods for Determination of Fracture Toughness of Advanced Ceramics at Ambient Temperature," *Annual Book of ASTM Standards, Vol. 15.01*, ASTM, West Conshohocken, PA (2001).
21. S.R. Choi, A. Chulya, and J.A. Salem, "Analysis of Precracking Parameters for Ceramic Single-Edge-Pre-cracked-Beam Specimens, pp. 73–88 in *Fracture Mechanics of Ceramics*, Vol. 10, Edited by R. C. Bradt, D. P. H. Hasselman, D. Munz, M. Sakai, and V.Ya. Shevchenko," Plenum Press, New York, NY (1992).
22. R.F. Krause, "Rising Fracture Toughness from the Bending Strength of Indented Alumina Beams," *J. Am. Ceram. Soc.*, **71**[5] 338–343 (1988).
23. P. Chantikul, G.R. Anstis, B.R. Lawn, and D.B. Marshall, "A Critical Evaluation of Indentation Techniques for Measuring Fracture Toughness: II. Strength Method *J. Am. Ceram. Soc.*, **64**[9] 539–543 (1981).
24. S.R. Choi, J.E. Ritter and K. Jakus, "Erosion and Impact Behavior of Various Advanced Ceramics at Ambient and Elevated Temperatures," unpublished work, University of Massachusetts, Amherst, MA (1988).

REPORT DOCUMENTATION PAGE

Form Approved
OMB No. 0704-0188

Public reporting burden for this collection of information is estimated to average 1 hour per response, including the time for reviewing instructions, searching existing data sources, gathering and maintaining the data needed, and completing and reviewing the collection of information. Send comments regarding this burden estimate or any other aspect of this collection of information, including suggestions for reducing this burden, to Washington Headquarters Services, Directorate for Information Operations and Reports, 1215 Jefferson Davis Highway, Suite 1204, Arlington, VA 22202-4302, and to the Office of Management and Budget, Paperwork Reduction Project (0704-0188), Washington, DC 20503.

1. AGENCY USE ONLY (<i>Leave blank</i>)		2. REPORT DATE August 2002	3. REPORT TYPE AND DATES COVERED Technical Memorandum	
4. TITLE AND SUBTITLE Foreign Object Damage Behavior of Two Gas-Turbine Grade Silicon Nitrides by Steel Ball Projectiles at Ambient Temperature			5. FUNDING NUMBERS WU-708-31-13-00	
6. AUTHOR(S) Sung R. Choi, J. Michael Pereira, Lesley A. Janosik, and Ramakrishna T. Bhatt				
7. PERFORMING ORGANIZATION NAME(S) AND ADDRESS(ES) National Aeronautics and Space Administration John H. Glenn Research Center at Lewis Field Cleveland, Ohio 44135-3191			8. PERFORMING ORGANIZATION REPORT NUMBER E-13513	
9. SPONSORING/MONITORING AGENCY NAME(S) AND ADDRESS(ES) National Aeronautics and Space Administration Washington, DC 20546-0001			10. SPONSORING/MONITORING AGENCY REPORT NUMBER NASA TM-2002-211821	
11. SUPPLEMENTARY NOTES Sung R. Choi, Ohio Aerospace Institute, Brook Park, Ohio, and NASA Senior Resident Research Scientist at Glenn Research Center; J. Michael Pereira, Lesley A. Janosik, and Ramakrishna T. Bhatt, NASA Glenn Research Center. Responsible person, Sung R. Choi, organization code 5920, 216-433-8366.				
12a. DISTRIBUTION/AVAILABILITY STATEMENT Unclassified - Unlimited Subject Categories: 07 and 39 Available electronically at http://gltrs.grc.nasa.gov This publication is available from the NASA Center for AeroSpace Information, 301-621-0390.			12b. DISTRIBUTION CODE	
13. ABSTRACT (<i>Maximum 200 words</i>) Foreign object damage (FOD) behavior of two commercial gas-turbine grade silicon nitrides, AS800 and SN282, was determined at ambient temperature through strength testing of flexure test specimens impacted by steel-ball projectiles with a diameter of 1.59 mm in a velocity range from 220 to 440 m/s. AS800 silicon nitride exhibited a greater FOD resistance than SN282, primarily due to its greater value of fracture toughness (K_{IC}). Additionally, the FOD response of an equiaxed, fine-grained silicon nitride (NC132) was also investigated to provide further insight. The NC132 silicon nitride exhibited the lowest fracture toughness of the three materials tested, providing further evidence that K_{IC} is a key material parameter affecting FOD resistance. The observed damage generated by projectile impact was typically in the forms of well- or ill-developed ring or cone cracks with little presence of radial cracks.				
14. SUBJECT TERMS Foreign object damage; FOD; Turbine-grade silicon nitrides; Impact testing; Strength testing; Mechanical testing for ceramics; Strength degradation due to FOD			15. NUMBER OF PAGES 25	
			16. PRICE CODE	
17. SECURITY CLASSIFICATION OF REPORT Unclassified	18. SECURITY CLASSIFICATION OF THIS PAGE Unclassified	19. SECURITY CLASSIFICATION OF ABSTRACT Unclassified	20. LIMITATION OF ABSTRACT	